# Óriás mágneses ellenállás (kísérleti)

1. Bevezetés – történelem

2. AF beállás Fe/Cr/Fe 3-rétegen (P. Grünberg)
   - Magyarázat: RKKY

3. $\Delta\rho/\rho(B=0)$ = – 50% (Fert)
   - Irányfüggetlenül

4. AMR – a GMR más eredetű
   - Mott modell (Cu, ill. Pd)
   - GMR két áram modellje

5. Struktúrák
   - Spinszelep, stb.
   - ~~Csatolás~~ – AF beállás ✓

6. Alkalmazások:
   - szenzorok és olvasófejek
   - DRAM

# EXCHANGE COUPLING AND GMR

in MAGNETIC/NON-MAGNETIC NANOSTRUCTURES (giant magneto-resistance)

**1986** → FM / NM / ← FM

ANTIFERROMAGNETIC ALIGNMENT OF FM LAYER MAGNETIZATION IN FM/NM/FM SANDWICHES, MULTILAYERS

↑ non-magnetic spacer mediating an exchange coupling between ferromagnetic layers **(RKKY)**

Fe/Cr/Fe : Grünberg (Jülich)

$[Gd/Y]_N$ : Majkrzak (Brookhaven)

**1988** $[Fe(3\,nm)/Cr(0.9\,nm)]_{60}$ Fert (Orsay)

4.2K: $\frac{\Delta\rho}{\rho(H=0)} \approx -50\%$ "GIANT" MAGNETORES. due to strong spin-dependent scattering

Bulk FM: $\Delta\rho/\rho \approx \pm 2\%$ : ANISOTROPIC MR

MR RATIO: $[R(H)-R(H=0)]/R(H=0) = \frac{\Delta R}{R} = \frac{\Delta\rho}{\rho}$

**1990** Oscillatory exchange coupling and GMR in FM/NM multilayers as a function of NM spacer thickness

Co/Ru, Co/Cr, Fe/Cr : Parkin (IBM)

Co/Cu : $\Delta\rho/\rho \approx 50\%$ at $T = 300K$ (Fert '91)

**1992** GMR in granular metals ≈ as high as in multilayers

Cu(Co) : Berkowitz (UCSD)

Ag(Co) : Chien (Baltimore)

Cu(Co), Ag(Co) solid solution —heat treatment→ Co prec.

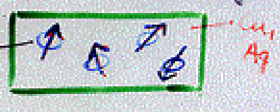


**1994** CPP GMR in multilayered nanowires

(ED: 1993) Schwarzacher/Bristol

current →

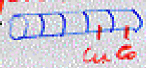


**1994** "Colossal" magnetoresistance (CMR) in perovskite oxides $La_{0.67}Ca_{0.33}MnO_{3+\delta}$

T≈300K: $\Delta R/R$ high but in very high fields only

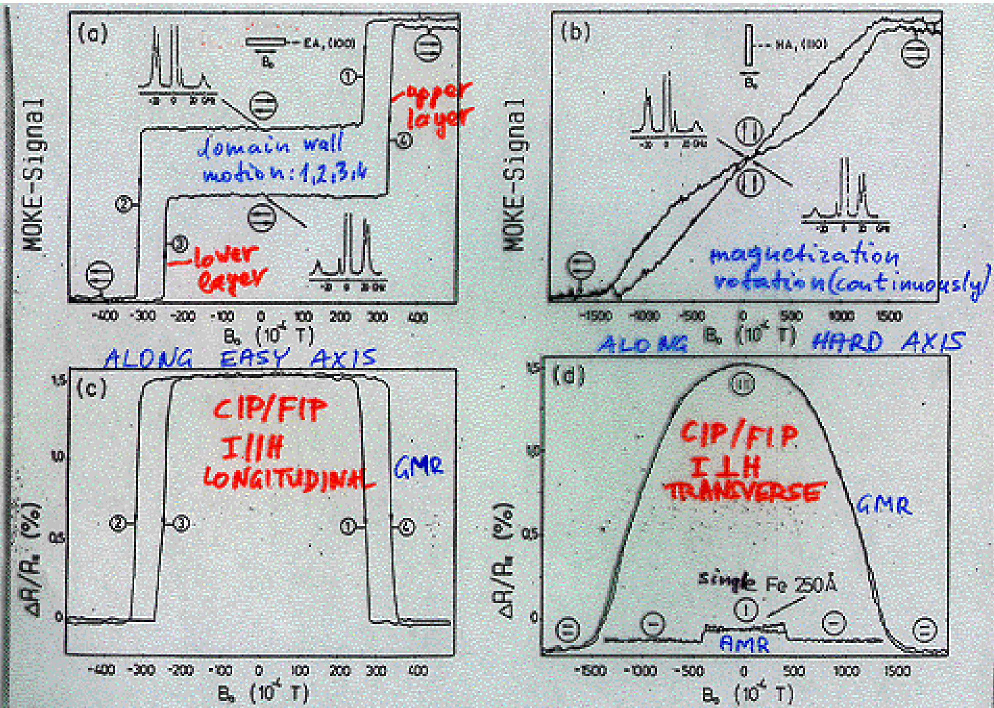


FIG. 2. (a)–(b) MOKE hysteresis curves and (c)–(d) magnetoresistance $\Delta R/R_s = (R - R_s)/R_s$ from Fe double layers with antiferromagnetic coupling. Also, (d) displays the anisotropic MR effect of a 250-Å-thick Fe film.

Fe(12 nm)/Cr(1 nm)/Fe(12 nm)

G. Binasch, P. Grünberg, F. Saurenbach, W. Zinn, PRB 39, 4828 (1989)

Ashcroft - Mermin : SSP



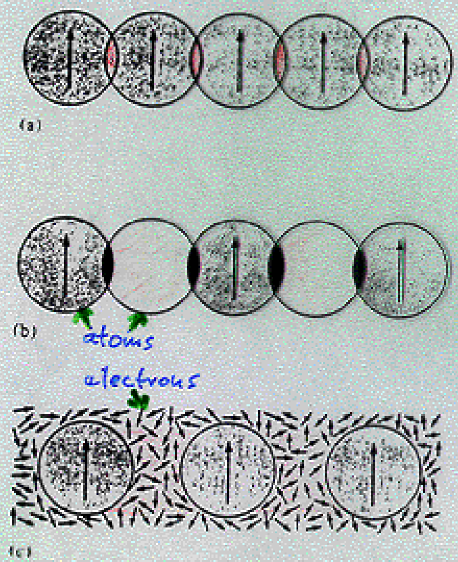


**Figure 32.2**
Schematic illustrations of (a) direct exchange, in which the magnetic ions interact because their charge distributions overlap; (b) super-exchange, in which magnetic ions with non-overlapping charge distributions interact because both have overlap with the same non-magnetic ion; and (c) indirect exchange, in which in the absence of overlap a magnetic interaction is mediated by interactions with the conduction electrons.

RKKY

# RKKY INTERACTION

Ruderman-Kittel-Kasuya-Yosida

Spin polarization of conduction electrons around a localized magnetic moment in a metal

Exchange interaction energy

$E = -J(r)\,\underline{\sigma}\,\underline{S}$  σ: conduction electron spin; S: magnetic moment

For $J(0) > 0$: $\uparrow_\sigma \uparrow_S$ alignment preferred

⇝ $\uparrow_\sigma$ electrons pile up at $r=0$

⇝ constructive interference of $\uparrow_\sigma$ states at $r=0$


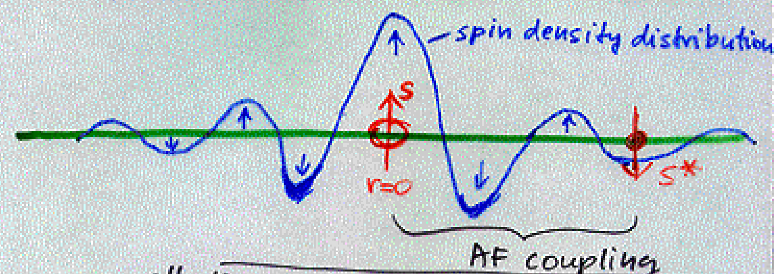


– oscillating spinpolarization
(but: homogeneous charge density distr.)

– for large r: $V(r) \propto \frac{\cos(2k_F r)}{r^3}$

– depending on separation: AF/FM coupling between localized magnetic moments mediated by conduction electrons

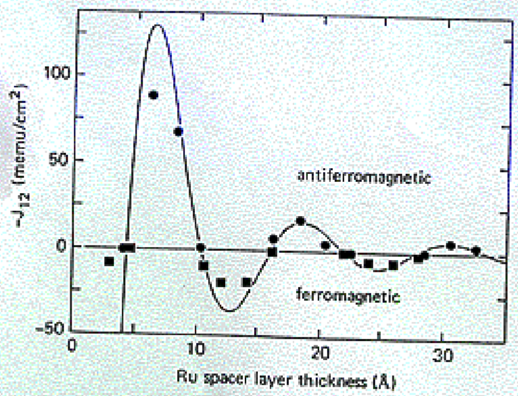


**Fig. 2.63.** Interlayer exchange coupling strength, $J_{12}$, for coupling of $Ni_{80}Co_{20}$ layers through a Ru spacer layer. $J_{12}$ is defined per unit area of the interface and is determined from magnetization curves of structures of the form **(a)** Si/Ru(85 Å)/[Co(15 Å)/Ru(6 Å)/$Ni_{80}Co_{20}$(15 Å)/Ru($t_s$)/$Ni_{80}Co_{20}$(15 Å)]$_5$ for *ferromagnetic* coupling, and **(b)** Si/Ru(105 Å)[$Ni_{80}Co_{20}$(30 Å)/Ru($t_{Ru}$)]$_{20}$/Ru(105 Å) for *antiferromagnetic coupling*. The data points are shown as **(a)** squares and **(b)** circles. For each structural type only (a) *ferromagnetic* or **(b)** *antiferromagnetic* coupling can be measured. Data points are not shown for structures for which no coupling could be determined. The solid line corresponds to a fit to the data of a RKKY form

## Mágneses $ML^{3L}$, indirekt csatolás : RKKY

(Y. Yafet, PRB 36, (1987) 3948 — RE/Y ML)

$$H_{eff}^{dd}(\rho) = \frac{J_{lc}^2 m_e Q^4 F(2Q\rho_{ij}) \underline{S}_i \underline{S}_j}{2\pi \quad 3\hbar^2}$$

$J_{lc}, \rho_{ij}, Q, m_e, \underline{S}_i \underline{S}_j$

$$F(x) = \frac{x \cdot \cos x - \sin x}{x^4} \sim \chi$$

→ $\int H_{eff}(\rho)\,d\rho = -J_1 \cdot \cos\theta(\underline{M}_i, \underline{M}_j)$

→ $F(\rho)$ oszcillál, ha $d \sim \pi/Q_F$

Mj: $H_{eff}^{dd}$ "kontakt" ha:

- $H^{sd} \to \underline{Q} = \underline{k} - \underline{k}'$
- d nívó nem degenerált

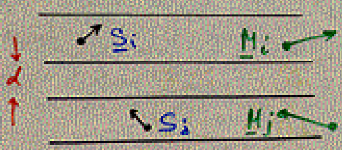

## QW fém köztesréteg:

$$J_1 = \left(\hbar^2 Q^2 / 4\pi^2 m_e w^2\right)(\Delta R)^2 \sin(2Qw)\,(\xi/\sinh\xi)$$

$$\xi = 2\pi k_B T w m_e / \hbar^2 Q$$

## QW szigetelő köztesréteg:

$$J_1(T=0) = \mathcal{J}(\kappa, x)$$

$$x = 2\pi k_B T w m_e / \hbar^2 \kappa$$

$$J_1(T>0) = J_1(T=0)\, x / \sin x$$

$$Q \rightarrow i\kappa$$

$$J_1(\text{fém}) \longleftrightarrow J_1(T>0, \text{szigetelő})$$

Fém: $J_1(w)$ oszcillál — Fe/Cr, Co/Cu

Szigetelő: $J_1(w)$ exp lecseng — Fe/Si, Fe/FeSi

# EXCHANGE COUPLING AND GMR

in MAGNETIC/NON-MAGNETIC NANOSTRUCTURES (giant magneto-resistance)

**1986** → FM / NM / ← FM — ANTIFERROMAGNETIC ALIGNMENT OF FM LAYER MAGNETIZATION IN FM/NM/FM SANDWICHES, MULTILAYERS

Fe/Cr/Fe : Grünberg Jülich

$[Gd/Y]_N$ : Majkrzak Brookhaven

↑ non-magnetic spacer mediating an exchange coupling between ferromagnetic layers **(RKKY)**

→ **1988** $[Fe(3\,nm)/Cr(0.9\,nm)]_{60}$ Fert (Orsay)

4.2K: $\frac{\Delta\rho}{\rho(H=0)} \approx -50\%$ "GIANT" MAGNETO[illegible]

due to strong spin-dependent [illegible]

Bulk FM: $\Delta\rho/\rho \approx \pm 2\%$ : ANISOTROPIC MR

MR RATIO: $[R(H)-R(H=0)]/R(H=0) = \frac{\Delta R}{R} = \frac{\Delta\rho}{\rho}$

**1990** Oscillatory exchange coupling and GMR in FM/NM multilayers as a function of NM spacer [illegible]

Co/Ru, Co/Cr, Fe/Cr : Parkin (IBM)

Co/Cu : $\Delta\rho/\rho \approx 50\%$ at T=300K (Fert '3[illegible]

**1992** GMR in granular metals ≈ as high as in multilayers

Cu(Co) : Berkowitz (UCSD)

Ag(Co) : Chien (Baltimore)

Cu(Co), Ag(Co) solid solution —**heat treatment**→ Co prec.

**1994** CPP GMR in multilayered nanowires

(ED: 1993)

Schwarzacher/Bristol

current →

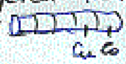


**1994** "Colossal" magnetoresistance (CMR) in perovskite oxides $La_{0.67}Ca_{0.33}MnO_{3+\delta}$

T≈300K: $\Delta R/R$ high but in very high fields only

M.N. Baibich, J.M. Broto, A. Fert et al., PRL 61, 2472 (1988)

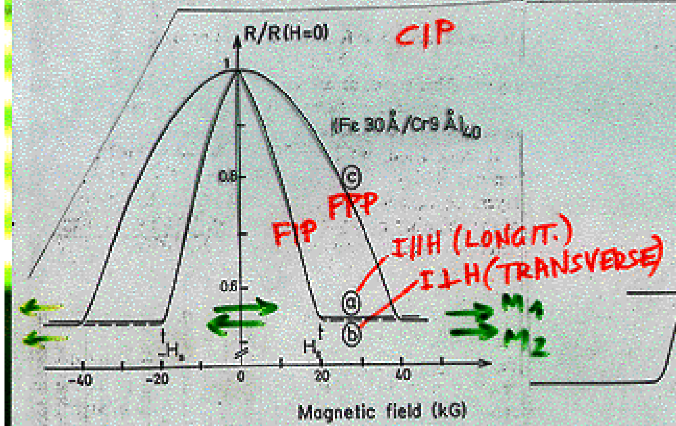


FIG. 2. Magnetoresistance of a [(Fe 30 Å)/(Cr 9 Å)]$_{40}$ superlattice of 4.2 K. The current is along [110] and the field is in the layer plane along the current direction (curve *a*), in the layer plane perpendicular to the current (curve *b*), or perpendicular to the layer plane (curve *c*). The resistivity at zero field is 54 μΩ cm. There is a small difference between the curves in increasing and decreasing field (hysteresis) that we have not represented in the figure. The superlattice is covered by a 100-Å Ag protection layer. This means that the magnetoresistance of the superlattice alone should be slightly higher.

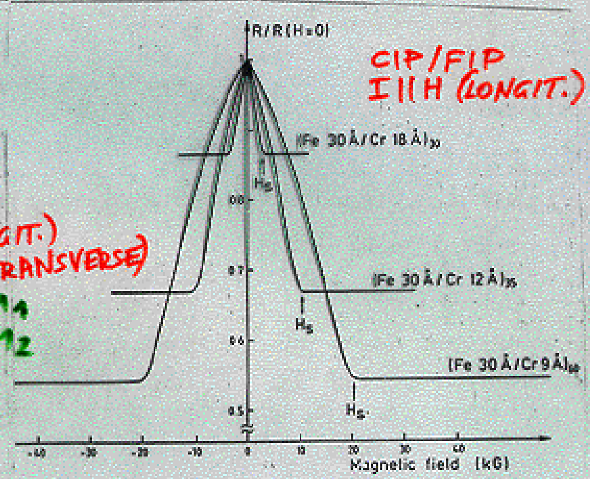


FIG. 3. Magnetoresistance of three Fe/Cr superlattices at 4.2 K.

The current and the applied field are along the same [110] axis in the plane of the layers.

# GMR IN MULTILAYERS

spin-dependent electron scattering leads to:

$\rho_{\uparrow\uparrow} < \rho_{\uparrow\downarrow}$

fulfilled only if electron mean free path long enough

$\lambda_{el} >> d_{FM}, d_{NM}$.

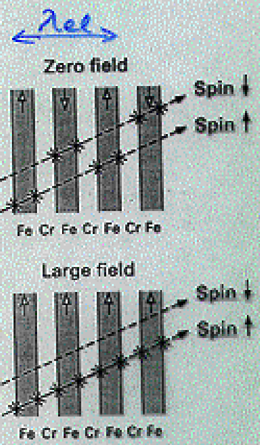


*Fig. 3 – Two-current model: schematic illustration of electron scattering at the interfaces in Fe/Cr multilayers with antiferromagnetic interlayer exchange coupling. Dashed lines are electron trajectories and fanned arrows indicate relatively large diffusive scattering probabilities at the interfaces; arrows in the Fe layers indicate the magnetization directions. The probability for diffusive scattering at an interface with magnetization "up" is much larger for spin-up than for spin-down electrons, and vice versa if the magnetization direction of the Fe layer is "down".*

For $\lambda_{el} \simeq d_{FM}, d_{NM}$:
progressive decoupling of the scattering processes in successive layers
⇝ GMR decreases

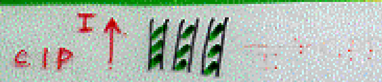


GMR(CIP) < GMR(CPP)

Effect of temperature

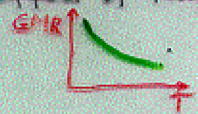


decrease due to increasing spin-mixing of the ↑ and ↓ electron channels, i.e., $\frac{\rho_\uparrow}{\rho_\downarrow} \to 1$

primarily due to collisions between electrons and spin fluctuations (magnons) in the FM layer

spin-dependent scattering:
- at interfaces (mainly)
- in bulk?

ANISOTROPIC MAGNETORESISTANCE (AMR) IN BULK, HOMOGENEOUS FERROMAGNETICS

1. Low fields ($H < H_s$)
2. High fields ($H > H_s$)
3. $\rho_{\parallel} \neq \rho_{\perp}$ (AMR)

Bozorth (1951)

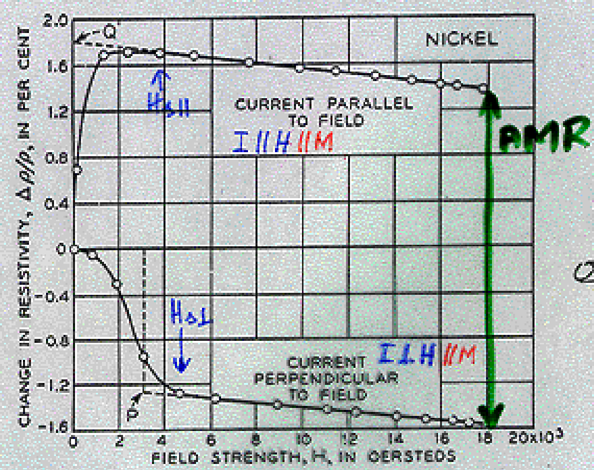


FIG. 16-7. Change of resistance of nickel in longitudinal and in transverse fields.

T = 300 K

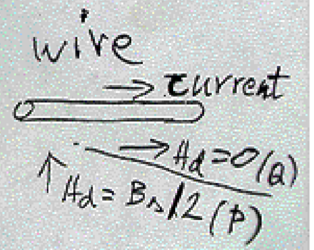

IEEE Trans. Magn. 11, 1018 (1975)



IN FM 3d ALLOYS

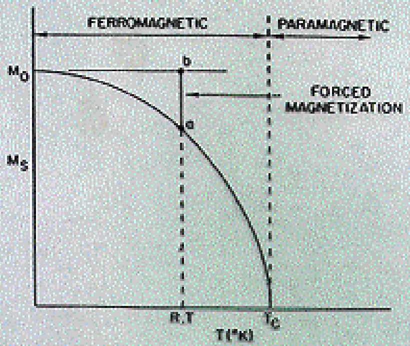


Fig. 1a. Variation of saturation magnetization $M_s$ with temperature. The line *ab* marks the region of forced magnetization at room temperature. It is this additional magnetization as a function of applied field that causes the corresponding decrease in the magnetoresistance, as indicated in Fig. 1b.

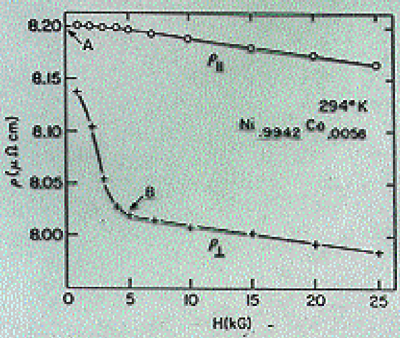


Fig. 1b. Resistivity of $Ni_{0.9942}Co_{0.0058}$ as a function of applied magnetic field at room temperature. The points *A* and *B* mark the selection of $\rho_\parallel$ and $\rho_\perp$ to determine the anisotropic magnetoresistivity associated with the orientation of the spontaneous moment $M_S$. The point *B* is at a higher applied field than *A* because of demagnetization.

J.Tóth et al., JMMM 198-199, 243 (1999)

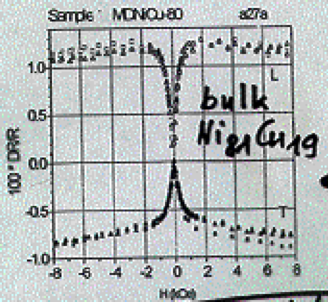


Field-dependence of
*electrodeposited* **$Ni_{81}Cu$**
*non-magnetic spacer lay*
*(Left upper corner, sa*

Configuration: current

**L**: longitudinal magne

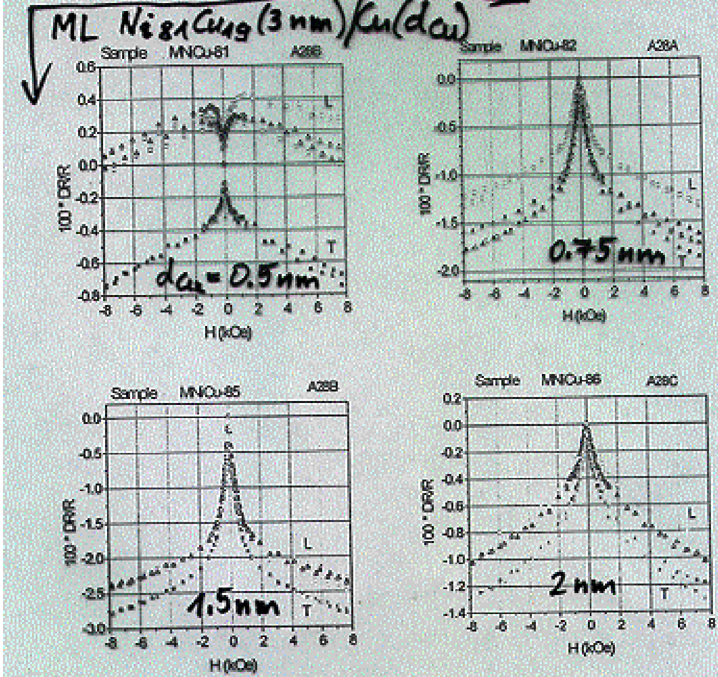

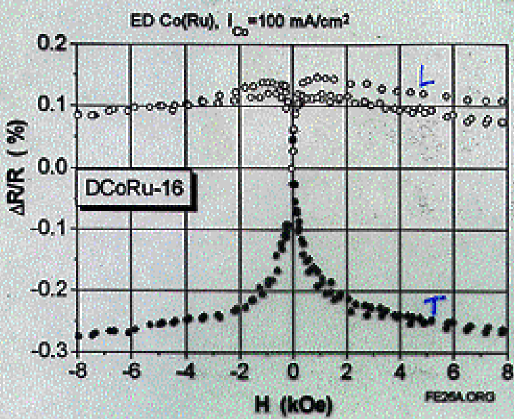


AMR

E.D ML Co/Ru(Cu)

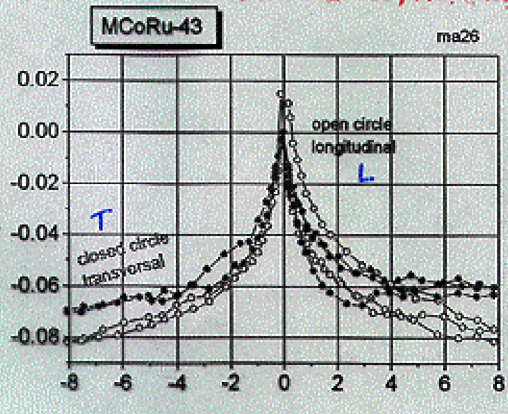


GMR

ELECTRICAL CONDUCTION IN METALS: mainly s (p) electrons are current carriers

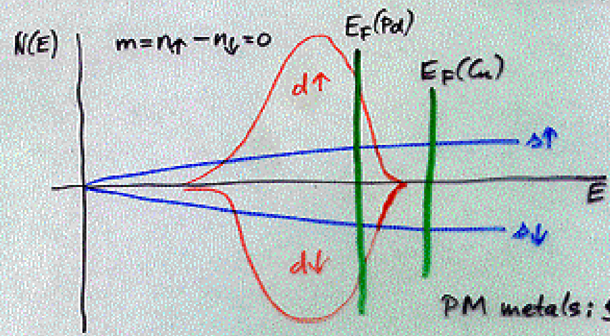


PM metals: $\rho_{s\uparrow} = \rho_{s\downarrow}$

Transition metals: s → d scattering

Mott model: $\rho_s \propto N_d(E_F)$

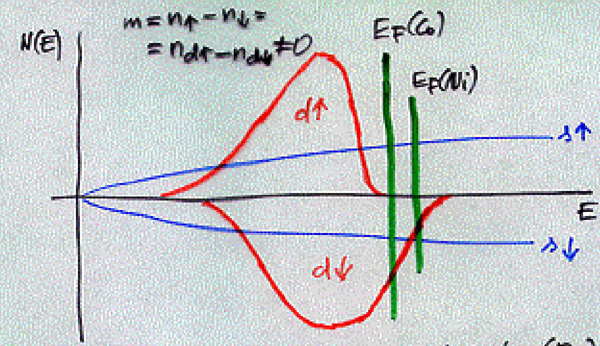


FM metals : $N_{d\uparrow}(E_F) \neq N_{d\downarrow}(E_F)$

Fert & Campbell: two - current model:

conduction in parrallel by two independent current channels : ↑ and ↓

$\rho_{s\uparrow} \ll \rho_{s\downarrow}$

$(N_{d\uparrow} \ll N_{d\downarrow})$

in absence of spin mixing: $\rho = \frac{\rho_\uparrow \rho_\downarrow}{\rho_\uparrow + \rho_\downarrow}$

Fert & Campbell (1976)

$\rho_\downarrow \neq \rho_\uparrow$

## TWO-CURRENT MODEL

two independent charge carrier channels: $\uparrow$, $\downarrow$

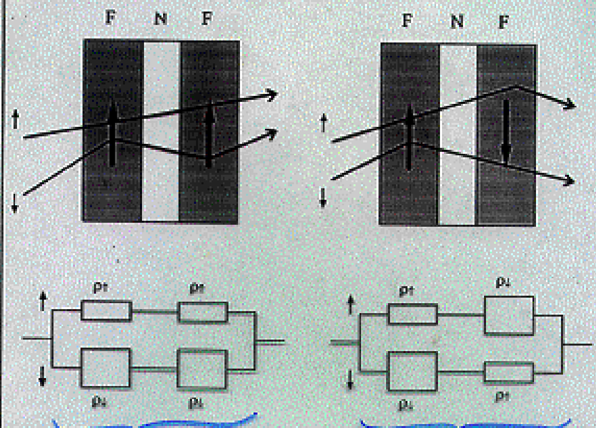


$\rho_{\uparrow\uparrow} (= \rho_{\downarrow\downarrow})$ $\rho_{\uparrow\downarrow} (= \rho_{\downarrow\uparrow})$

Az ábra a vezetési elektronoknak a GMR effektusért felelős spin-függő szórását szemlélteti. Az elektronok spin-irányát a kis nyíl ábrázolja, az adott konfigurációval ekvivalens ellenállás-elrendezést alul láthatjuk. Láthatóan minden egyes ferromágneses rétegben az elektronok egy része erősen szóródik (analóg képben nagy ellenállást jelent), másik része pedig gyengén (kis ellenállás). Az egész struktúrát tehát 4 db összekötött ellenállás reprezentálja. A parallel konfigurációban (bal oldali ábra) alacsonyabb eredő ellenállást kapunk, mint az antiparallel konfigurációban (jobb oldali ábra). Valójában az áram zöme a rétegek síkjában folyik, a rétegekre merőleges áramkomponenst a szemlélet kedvéért eltúloztuk.

Resistivity: spin dependent $\rho \to \rho_\downarrow, \rho_\uparrow$

$\rho_\uparrow = \rho(1-\beta)$ $\rho_\downarrow = \rho(1+\beta)$

$$\rho_{\uparrow\uparrow} = \frac{2\rho_\uparrow\rho_\downarrow}{\rho_\uparrow+\rho_\downarrow} = \rho(1-\beta^2) \qquad \rho_{\uparrow\downarrow} = \frac{\rho_\uparrow+\rho_\downarrow}{2} = \rho$$

$\rho_{\uparrow\uparrow} < \rho_{\uparrow\downarrow}$ $(\beta \geq 0)$

# EXCHANGE COUPLING AND GMR

in MAGNETIC/NON-MAGNETIC NANOSTRUCTURES   giant magneto resistance

**1986**   → FM / NM / ← FM   ANTIFERROMAGNETIC ALIGNMENT OF FM LAYER MAGNETIZATION IN FM/NM/FM SANDWICHES, MULTILAYERS

↑ non-magnetic spacer mediating an exchange coupling between ferromagnetic layers **(RKKY)**

Fe/Cr/Fe : Grünberg (Jülich)

$[Gd/Y]_N$ : Majkrzak (Brookhaven)

**1988**   $[Fe(3\,nm)/Cr(0.9\,nm)]_{60}$   Fert (Orsay)

4.2K: $\frac{\Delta\rho}{\rho(H=0)} \approx -50\%$   "GIANT" MAGNETORES...
due to strong spin-dependent ...

Bulk FM: $\Delta\rho/\rho \approx \pm 2\%$ : ANISOTROPIC MR

MR RATIO: $[R(H)-R(H=0)]/R(H=0) = \frac{\Delta R}{R} = \frac{\Delta\rho}{\rho}$

**1990**   Oscillatory exchange coupling and GMR in FM/NM multilayers as a function of NM spacer thickness

Co/Ru, Co/Cr, Fe/Cr : Parkin (IBM)

Co/Cu : $\Delta\rho/\rho \approx 50\%$ at $T = 300K$ (Fert '91)

→ **1992**   GMR in granular metals ≈ as high as in multilayers

Cu(Co) : Berkowitz (UCSD)

Ag(Co) : Chien (Baltimore)

Cu(Co), Ag(Co) solid solution —**heat treatment**→ Co prec.


**1994**   CPP GMR in multilayered nanowires
(ED: 1993) Schwarzacher/Bristol
current → 

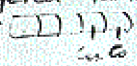


**1994**   "Colossal" magnetoresistance (CMR) in perovskite oxides $La_{0.67}Ca_{0.33}MnO_{3+\delta}$

T≈300K: $\Delta R/R$ high but in very high fields only

**3** Various GMR nanostructures (left) and their magnetoresistance behaviour (right – note that all the horizontal scales are different). (*a*) antiferromagnetically coupled multilayer; (*b*) spin-valve structure; (*c*) granular alloy; (*d*) multilayer with discontinuous magnetic layers; (*e*) hybrid nanostructure including clusters and layers. See text for details

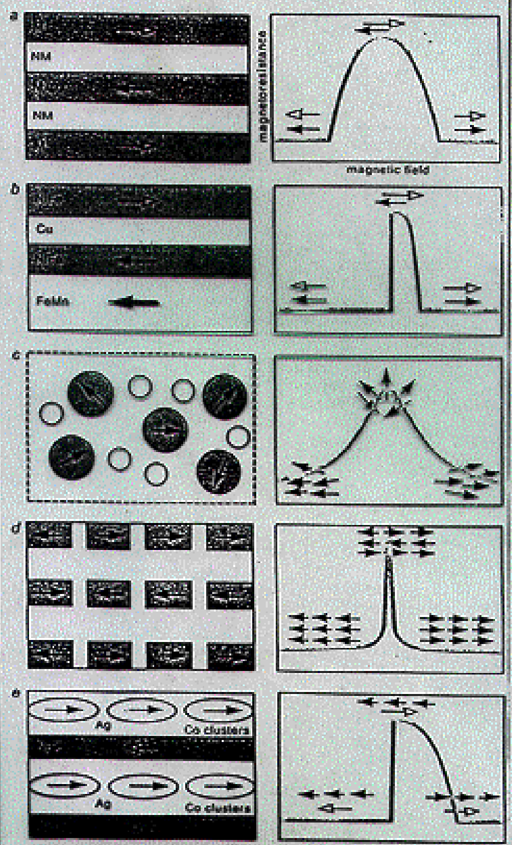

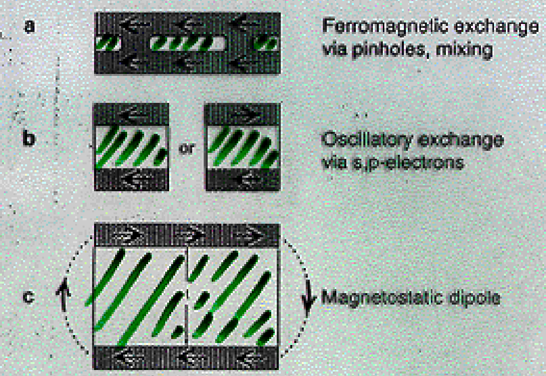


**Figure** 15. Coupling between magnetic layers (▦) via non-magnetic spacers of varying thickness $t$ (▨). (a) In the near-contact region, direct exchange dominates (usually ferromagnetic). (b) For spacer of a few nanometres, an oscillatory coupling is mediated by s, p electrons (RKKY interaction; see section 5.4 and figures 38–40). (c) At the largest distances, magnetic dipole interaction orients the layers antiparallel, like macroscopic bar magnets.

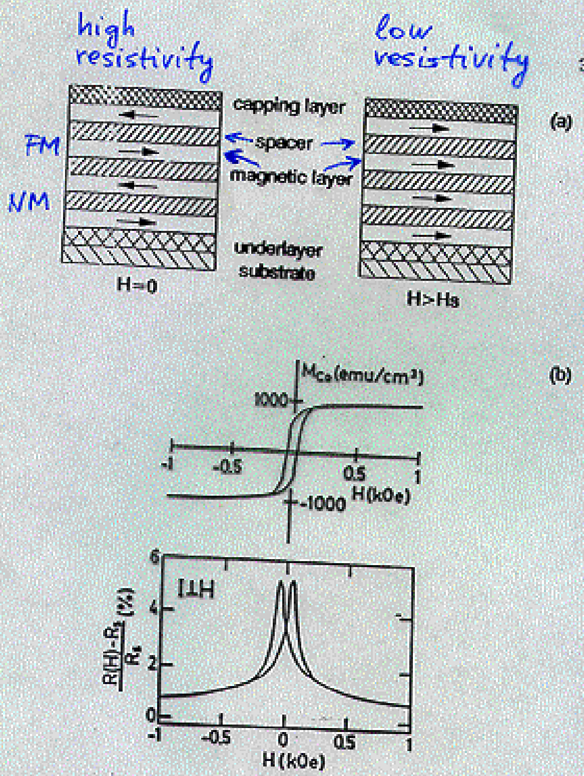


Figure 3. Antiferromagnetically coupled multilayer structure (a) in $H$=0 and in $H>H_{sat}$; (b) the corresponding magnetic field dependence of the magnetization and of the resistance for 30 bilayers of 17 Å Co/41 Å Cu deposited on an 50 Å thick Fe underlayer (from [22]).

Parkin et al., in: Magn. & Structure in Systems of Reduced Dimensions (1993), p. 113

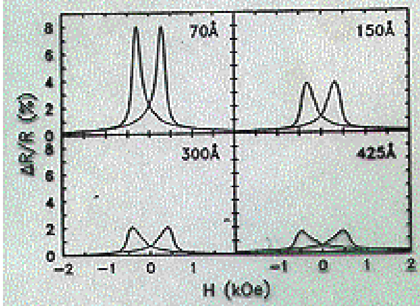


**Figure 4.** Resistance versus field curves for four Co/Cu multilayers of the form, Si(111)/Ru(50Å)/[Co(11Å)/Cu($t_{Cu}$)]$_6$ /Ru(15Å) with Cu spacer layer thicknesses, $t_{Cu}$, of 70, 150, 300 and 435 Å.

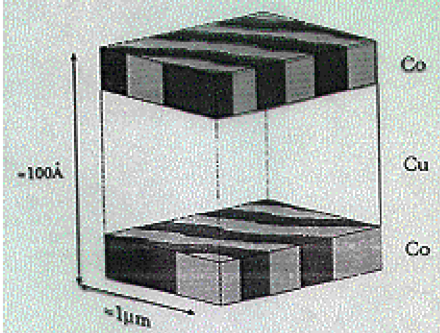


**Figure 5.** A schematic diagram of the arrangement of the magnetic domains in the remanent magnetic state of a Co/Cu multilayer. The darker and lighter shaded regions correspond to longitudinal magnetic domains aligned parallel and antiparallel to the magnetic field direction.

T. Shinjo, in: Magn. & Structure in Systems of Reduced Dimensions (1993), p. 323

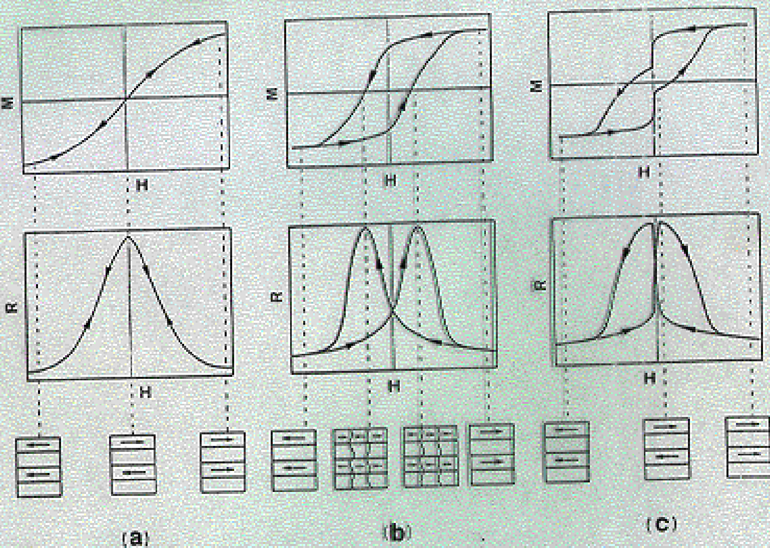


Fig.1. Schematic illustrations of magnetic hysteresis and magnetoresistance(MR) curves of multilayers,
(a) multilayers with strong antiferromagnetic coupling,
(b) the interlayer coupling is weakly antiferromagnetic,
(c) non-coupled type multilayers including two magnetic components with different coercive forces.

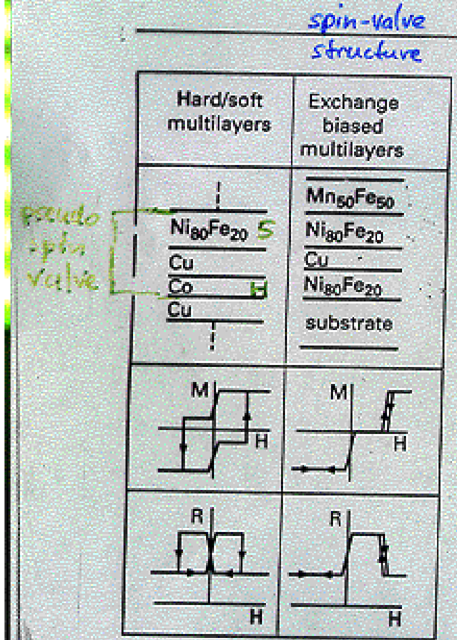


*Fig. 4 — Magnetoresistive multilayers with high sensitivity: a, upper) illustrations of hard/soft (left) and exchange-biased (right) systems which have been proposed, together with schematic representations of the magnetization M(H) and resistance R(H) responses in a magnetic field H.*
*b, lower) The corresponding experimentally observed room-temperature magnetoresistance: 30 x (2 nm Co/5 nm Cu/3 nm $Ni_{80}Fe_{20}$/5 nm Cu) hard/soft multilayer (left) and an exchange-biased (8 nm/2.5 nm Cu/6 nm $Ni_{80}Fe_{20}$/8 nm MnFe) multilayer (right).*

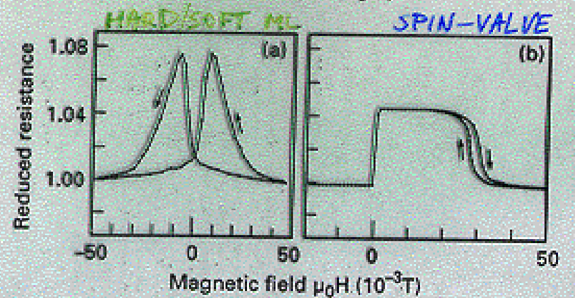

# Alkalmazások

1.) Mágneses szenzorok és olvasófejek

2.) Magnetorezisztív DRAM

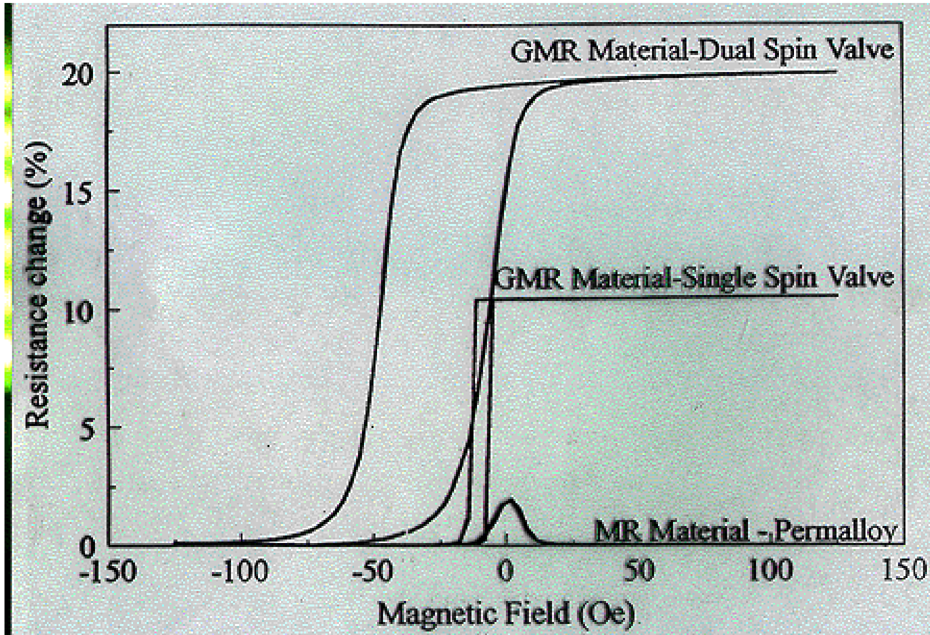


*Figure 2. Comparison of the response of permalloy, a spin-valve material, and a dual-spin valve material to a magnetic field. The response is for a sheet film except for the case of the MR response, for which a patterned bar was used to control the direction of the current.*

Figure 3. Magnetic Recording Process

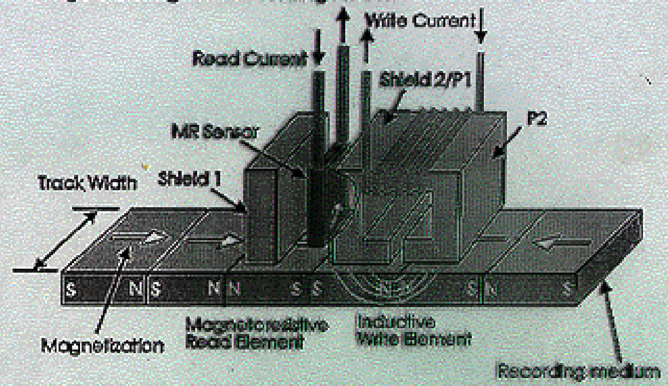


**Figure 3**, an idealized diagram of the magnetic recording process, depicts a merged MR head flying over a rotating disk. The inductive element writes bits of information as magnetically biased regions within radially concentric areas, or tracks, that are subsequently read by the MR sensor. The presence of a magnetic transition, or flux reversal, between bits causes the magnetization in the MR sensor to rotate. This rotation can be detected directly as a resistance change by a precision amplifier, which then produces the stronger signal that relays the information to the disk drive's electronics channel.

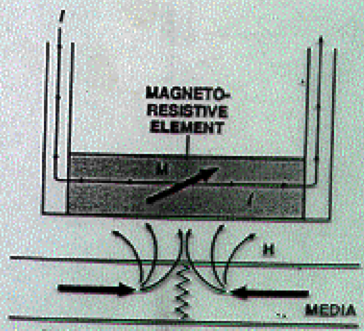


Fig. 1. Schematic of magnetoresistive "read" sensor

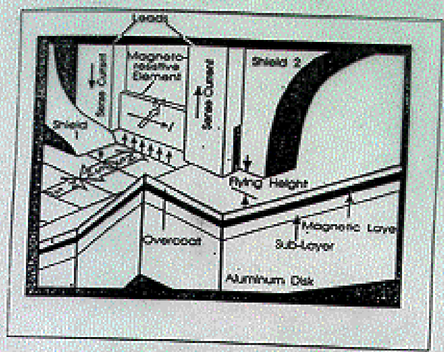


Fig. 3a. A conceptual cutaway view of a magnetoresistive read head.

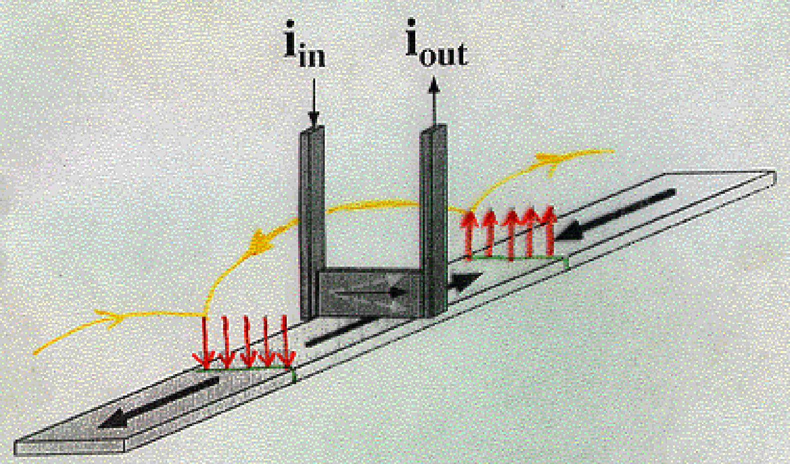


Fig. 1. Schematic representation of a GMR read head passing over recording media containing magnetized regions. The magnetization direction of the soft layer in the head responds to the fields emanating from the media by rotating either up or down. The resulting change in the resistance is sensed by the current passing through the GMR element.

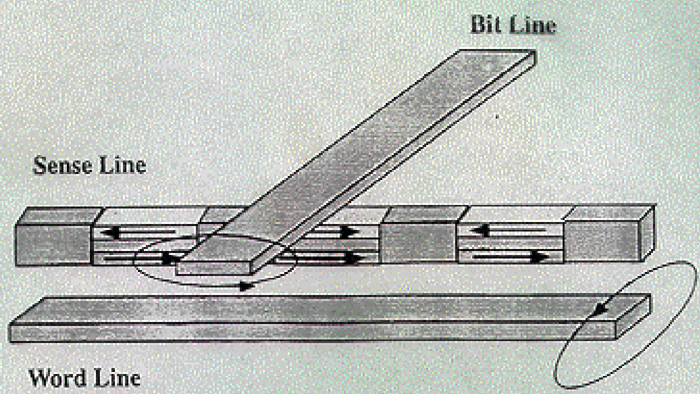


Fig. 5. Schematic representation of random access memory (RAM) constructed of GMR elements connected in series. They are manipulated, for writing or reading, by applying magnetic fields generated by currents passing through lines above and below the elements.

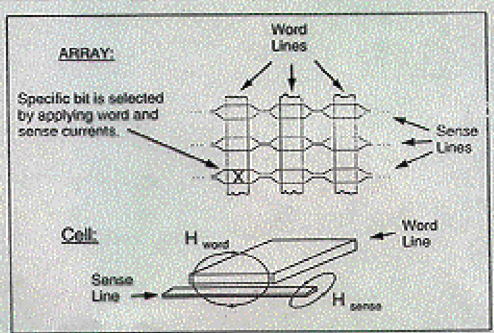


**Figure 2. Total magnetic field from word and sense current causes layers in sense line to rotate thereby changing resistance.**

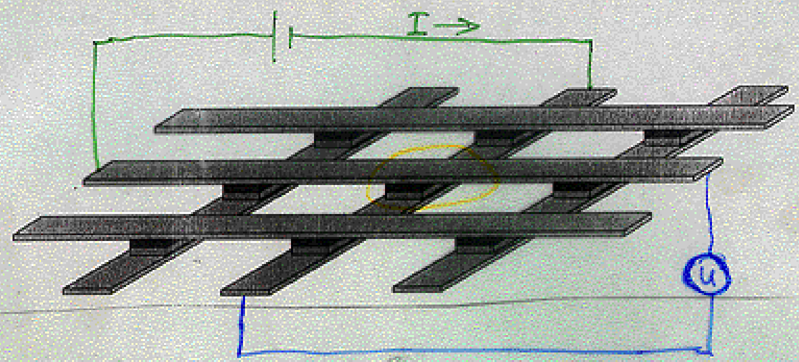


Fig. 7. Schematic representation of random access memory constructed of magnetic tunnel junctions connected together in a point contact array. The conducting wires provide current to the junctions and permit voltage measurements to be made. They also enable manipulation of the magnetization of the elements by carrying currents both above and below the magnetic junctions to create magnetic fields.

Stoner - Wolfart

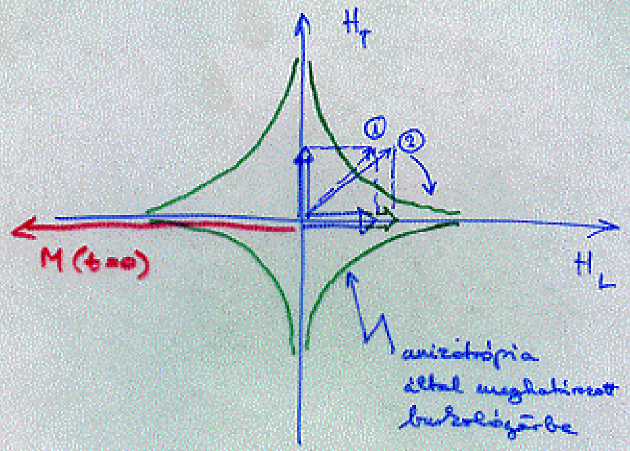


A 2 merőleges térrel (árammal) való forgatás sémája : ② helyzettől biztosan átbillen a mágnesezettség $+H_L$ irányába.

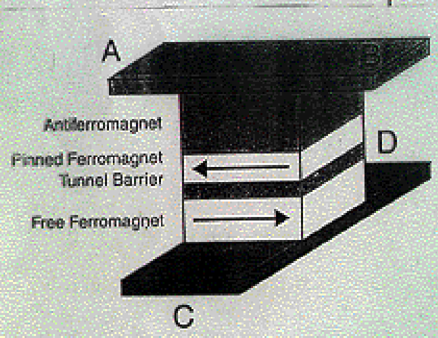


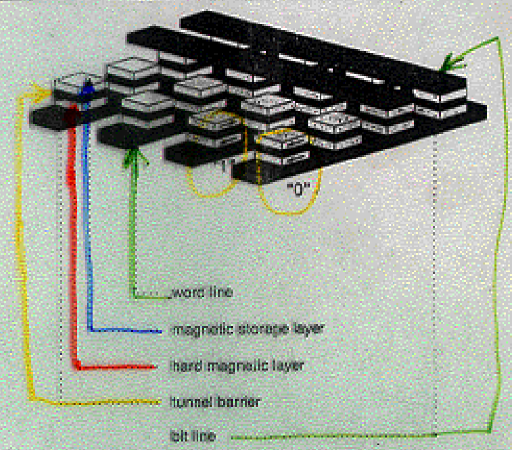


MRAM using magnetic tunnel junctions for bit storage

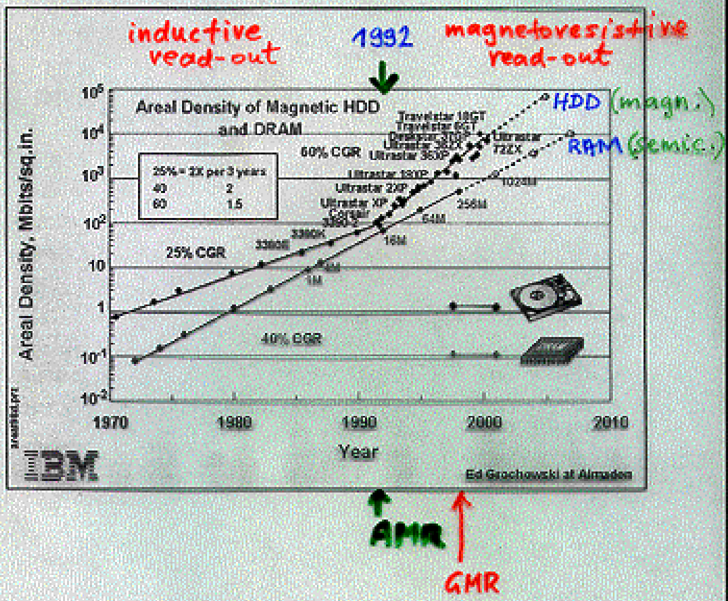
inductive read-out
1992
magnetoresistive read-out
Areal Density of Magnetic HDD and DRAM
HDD (magn.)
RAM (semic.)
25% = 2X per 3 years
40 2
60 1.5
60% CGR
25% CGR
40% CGR
Travelstar 18GT
Travelstar 6GT
Ultrastar 36XP
Ultrastar 18XP
Ultrastar 2XP
Ultrastar XP
Corsair
3380K
3380E
Ultrastar 72ZX
1024M
256M
64M
16M
4M
1M
Areal Density, Mbits/sq.in.
1970
1980
1990
2000
2010
Year
IBM
Ed Grochowski at Almaden
AMR
GMR